Editors' Suggestion

Radio-frequency-modulated artificial synapses based on magnetic tunnel junctions with perpendicular magnetic anisotropy

Kexin Zeng,[1,2] Yawen Luo,[3] Like Zhang,[4,*] Huayao Tu,[2] Yanxiang Luo,[2] Xuan Zhang,[2] Bin Fang,[1,2,†] and Zhongming Zeng[1,2,‡]

[1] *Nano Science and Technology Institute, University of Science and Technology of China, Hefei, Anhui 230026, People's Republic of China*

[2] *Nanofabrication Facility, Suzhou Institute of Nano-Tech and Nano-Bionics, CAS, Suzhou, Jiangsu 215123, People's Republic of China*

[3] *Department of Forest Conservation, Shanxi Agricultural University, Taiyuan, Shanxi 030031, People's Republic of China*

[4] *School of Electronics and Information Engineering, Wuxi University, Wuxi, Jiangsu 214105, People's Republic of China*

(Received 25 July 2023; revised 27 October 2023; accepted 11 December 2023; published 12 January 2024)

Magnetic-tunnel-junction- (MTJ) based spintronic devices have demonstrated significant potential in neuromorphic computing. Here, we report an artificial synapse, which can be modulated by rf signals directly based on the nanoscale MTJs with perpendicular magnetic anisotropy (PMA). To utilize multiple rf signals in parallel, we take an approach to change the resonance frequencies of MTJs by changing the PMA between the Co-Fe-B free layer and MgO barrier, which can expand the application range of rf signal processing. Moreover, we experimentally demonstrate that MTJs with PMA can serve as an rf synapse with adjustable positive and negative weights. We have achieved effective classification of rf signals with an accuracy exceeding 96% through experimental results as synaptic weights, comparable to that of equivalent software-based neural networks. This work may pave the way for the development of rf-oriented hardware artificial neural networks.

DOI: 10.1103/PhysRevApplied.21.014020

I. INTRODUCTION

Recently, spintronic devices with nonvolatility, outstanding read-write endurance, high-speed operation, and great scalability have demonstrated significant potential in neuromorphic computing [1–7], which mimics the functionalities involved in the neurons and synapses by utilizing hardware. As a representative spintronic device structure, nanoscale magnetic tunnel junctions (MTJs) have been found to be able to emulate synapses through various control mechanisms. For example, embedding MTJs within CMOS circuits can be used to store synaptic weights to achieve computing in memory [8–10]. Spintronic memristors based on MTJs can achieve nonvolatile and plastic synaptic weights through domain-wall motion, controlling the number of skyrmions, and so on [11,12]. The artificial synapses based on MTJs can implement spike-timing-dependent plasticity by utilizing stochastic magnetization switching or changing the skyrmion density [13,14]. More recently, Leroux *et al.* proposed an alternative computing paradigm using spin-torque diode effect, which could process multiple analog rf inputs in parallel and perform the multiply accumulate (MAC) operation without conversion between digital and analog signals [15–18]. The work has provided a way to utilize rf signals by building a computing paradigm based on MTJ devices. According to the principle of spin-torque diode effect [19,20], the spin torque arises from a microwave current inducing a small oscillation of the magnetization of the free layer around its steady state, and the MTJ emits a dc voltage when the frequency of the rf current is close to the eigenfrequency of the nanomagnetization oscillation. Besides, Leroux *et al.* theoretically have proven that the output dc voltage is proportional to the input rf power injected into the MTJs, and it can be expressed as $v_i = P_i\omega_i$, where v_i is the observed peak-to-peak voltage in spin-torque ferromagnetic resonance (STFMR) response for an external rf power of P_i, and the synaptic weight $\omega_i = \omega_i(f_i^{\mathrm{rf}} - f_i^{\mathrm{res}})$ is a function of the difference between the resonance and input frequencies, which can be controlled by changing the resonance frequency of spin-torque diode [15–18]. It is worth noting that in order to achieve

*lkzhang@cwxu.edu.cn
†bfang2013@sinano.ac.cn
‡zmzeng2012@sinano.ac.cn

processing multiple analogue microwave inputs in parallel, the injected microwave signal frequency needs to be fixed, and different frequencies of microwave signals need to be received and processed by MTJs with corresponding response frequencies to keep frequency multiplexing. To demonstrate the theoretical proposal, they realized experimentally diverse response frequencies through tuning the size- and shape-based MTJ with magnetic vortex or pushing the vortex core away from the center of the dot by Oersted field [16]. However, the response frequency of MTJs with the magnetic vortex states is relatively low [21–23], which limits the range of rf signal. In order to process signals with different response frequencies, a number of devices with different sizes need to be fabricated to construct a neural network, which is hard to control and is not conducive to miniaturization.

In this work, we demonstrate that the resonance frequencies can be tailored via the interfacial engineering of the perpendicular magnetic anisotropy (PMA) between the oxide and the ferromagnetic metal (Co-Fe-B/MgO) of nanoscale MTJs, in order to keep frequency multiplexing and expand the application range of rf signal processing. Moreover, the MTJs with PMA can be implemented with the same material stack used to produce spin-transfer torque magnetic random-access memory, which is able to achieve computing in memory, and hence is going to be fully CMOS compatible. In such systems, the interfacial PMA is attributed to the hybridization of O 2*pz* and Fe 3*dz* orbitals [24–27] and can be controlled by the free-layer thickness [28–30]. It is easier to obtain the varied resonance frequencies by fine control of the free-layer thickness in sample preparation. We experimentally demonstrate that MTJs with PMA can be used as rf synapses with tunable positive and negative weights, as well as perform an artificial neural network (ANN) on analog rf signals by using MTJs as synapses, classifying three-pixel encoded data into three categories with over 96% accuracy, equivalent to the software neural networks. Our work may provide inspiration to embedded rf artificial intelligence.

II. METHODS

A. Experiments

The multilayer stacks of three typical MTJs with different Co-Fe-B free-layer thicknesses are as follows: bottom electrode/Ta(5)/Co-Fe-B(t)/MgO(0.88)/Co-Fe-B(3)/Ru (0.85)/CoFe(2.3)/PtMn(15)/top electrode. The numbers in parentheses are the layer thicknesses in nanometers, where the Co-Fe-B free-layer thicknesses of devices *A*,*B*,*C* $t_{Co-Fe-B}$ are 1.63, 1.67, and 1.72 nm, respectively. The bottom Co-Fe-B free layer is designed to control PMA precisely [31,32]. The magnetic layers were deposited by magnetron sputtering and then annealed at 300 °C for 2 h in a magnetic field of 1 T. Electron-beam lithography and ion-beam milling were used to pattern the MTJ layer into elliptical nanopillars, where the dimensions of all three devices were 60 × 210 nm^2 and the long axis was along the annealing field direction. The ground-signal-ground (*G*-*S*-*G*) electrodes were fabricated by ultraviolet lithography and electron-beam evaporation. Figure 1(a) depicts the structure of MTJs and the measurement setup. The spin-torque ferromagnetic resonance (STFMR) measurement was performed under an in-plane magnetic field along the magnetization hard axis of MTJ (corresponding to the short axis of an elliptical nanopillar), which was the same as our previous work [30,31]. The rf current was generated by a signal generator (Keysight N5183B) and then applied to the device through a bias tee. The rectified voltage through the spin-torque diode effect was measured by a nanovoltmeter. All the data showed below were measured at room temperature.

III. RESULTS AND DISCUSSION

The static transport properties of the devices were firstly characterized. Figure 1(b) shows the magnetoresistance

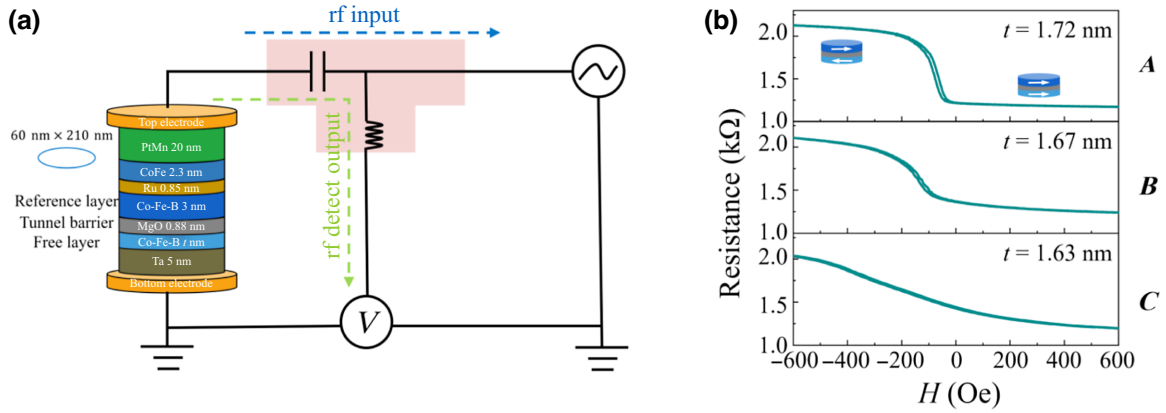

FIG. 1. (a) Device geometry and measurement configuration. (b) The MR curves of devices *A*, *B*, and *C* under the in-plane magnetic field.

(MR) of the three devices as a function of the applied magnetic field along the elliptical long-axis direction, with an applied bias current of 10 μA. Obviously, the MR curves transit gradually from a square loop to a smoother one as $t_{Co-Fe-B}$ decreases, which indicates a transition of the magnetization direction of the Co-Fe-B free layer from in-plane to out-of-plane orientation [29,32]. For device A in Fig. 1(b), it can be seen that the resistance displays a pronounced transition as a function of the magnetic field with a tiny hysteretic behavior, which is typical of a system with an in-plane easy axis. As $t_{Co-Fe-B}$ is reduced, the transition from the high-resistance state to the low-resistance state gradually turns smooth and it is no longer hysteretic as shown for device B in Fig. 1(b). The system clearly exhibits a slight tilting of the magnetization out of the plane due to the addition of PMA, although the easy axis is generally in plane. For the thinnest free layer, the curve of device C is smoother than other devices, which demonstrates the magnetization of Co-Fe-B free layer is further tilted towards the out-of-plane direction and it requires a stronger magnetic field to saturate it parallel to the in-plane direction. The observed changes from Fig. 1(b) indicate a modulation of the PMA in devices A, B, and C.

Next, we tested the STFMR curves of the three typical devices under different magnetic field conditions (from −20 to +20 Oe) to verify that the MTJs with PMA can both respond to rf signals with different resonance frequencies and achieve MAC operation. Figures 2(a)–2(c) show the detection voltages (V_{dc}) of devices A, B, and C as a function of input rf frequency at an rf input power of 10 μW ($P_{rf} = 10\ \mu$W) without applying dc bias current under different fields. It is apparent that the resonance frequency changes as the free-layer thickness varies. Besides, it is noted that there is a difference between the curves of device C and the curves of devices A and B that the positive peaks of devices A and B are in front, contrary to the curves of device C. In general, the STFMR lineshape can be well described as a symmetric and antisymmetric Lorentzian. The STFMR can be fitted by the Lorentz function as follows [33–36]:

$$V_{dc} = V_A \frac{4(f_r - f)\Delta f}{4(f_r - f)^2 + \Delta f_s^2} + V_s \frac{\Delta f^2}{4(f_r - f)^2 + \Delta f_s^2} + V_c, \tag{1}$$

where Δf is the full width at half maximum, f_r is the resonant frequency, and V_A and V_S are the amplitudes of antisymmetric and symmetric Lorentzian.

V_A changes sign when the relative angle φ between the free layer and the reference-layer magnetization changes from obtuse to acute due to $V_A \propto \cos(\varphi)$ [37]. These devices have different angles φ due to the variability of the PMA. The angles φ at zero field are estimated to be 33.7°, 55.8°, and 91.2°, respectively, as calculated from the angle relationship of the MTJ resistance:$R^{-1}(\varphi) = [(1 + \cos\varphi)R_P^{-1} + (1 - \cos\varphi)R_{AP}^{-1}]/2$. It means that the antisymmetric part in device C is opposite to those in devices A and B. In other words, the lineshape depends on the angle of the free-layer magnetization vector projected on the sample plane and the reference-layer magnetization [38].

In addition, although the curves of device C are drastically different from devices A and B, they still consist of the symmetric and antisymmetric parts, both positive and negative synaptic weights of which can be obtained by changing the magnetic field. To acquire the resonance frequencies more precisely, we have fitted the experimental data by Eq. (1). The resonance frequencies of devices A, B, and C under zero magnetic field were found to be about 745, 955, and 1505 MHz, respectively. The result confirms that the modulation of interfacial PMA occurs with the $t_{Co-Fe-B}$, leading to a change in the resonance frequencies of the MTJs, which enables the MTJs with varied PMA to selectively respond to rf signals with different frequencies.

Subsequently, to verify that MTJs with PMA can perform the multiplication operations similar to MTJs with the magnetic vortex states, we fixed the magnetic field at zero-field conditions and changed the injected microwave power to test the response curves of devices A, B, and C under different microwave injection frequencies, as depicted in Figs. 2(d)–2(f). As the microwave power increases, the rectified voltage of the devices continuously increases. By extracting the rectified voltage values at different input frequencies, we can obtain the microwave response curves of the devices under different injected microwave frequencies, as shown in Figs. 2(g)–2(i). We notice that compared to devices A and B, the response of device C to different microwave powers is reverse, with the largest input frequency at the bottom rather than on the top. It is due to the different STFMR curve of C compared with devices A and B as shown in Figs. 2(a)–2(c). However, this does not affect the fact that device C can perform the multiplication operations as well as devices A and B, since for different fixed microwave input frequencies, the rectified voltage exhibits a good linear relationship with the input power, indicating that the synaptic weights are independent of the injected microwave power and the spin-torque diode effect can be used to perform multiplication operations in MTJs with PMA.

Additionally, it can be observed that as the magnetic field changes from −20 to +20 Oe, the resonance frequencies of the devices change slightly as shown in Figs. 2(a)–2(c). According to Kittel's formula [39], the resonance frequency of the MTJ is influenced by the applied magnetic field. Therefore, by appropriately adjusting the magnetic field magnitude, the response frequencies of the devices can be modulated while maintaining almost unchanged curve shape. It preliminarily confirms that our devices can tune synaptic weights by changing the

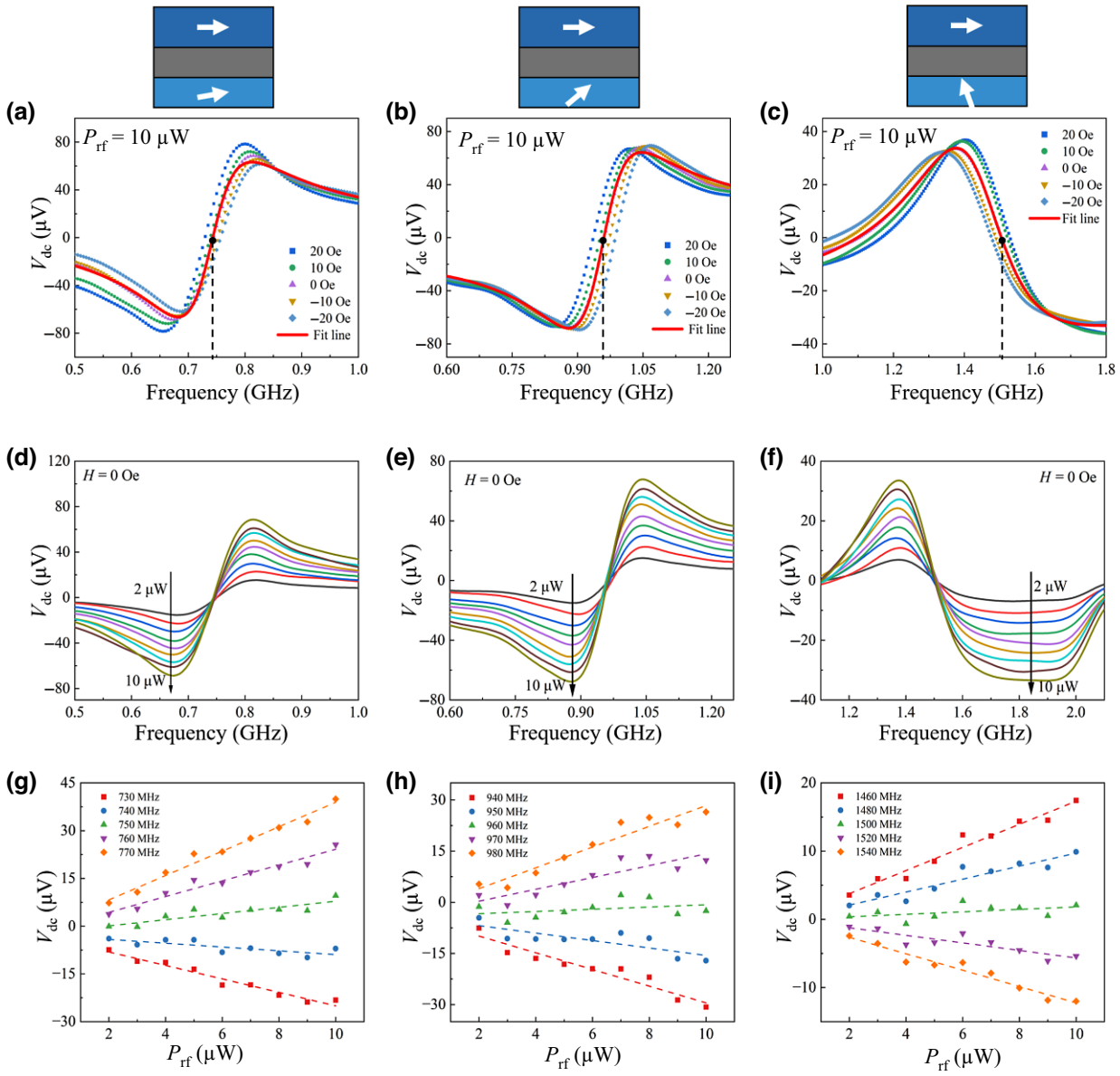

FIG. 2. (a)–(c) The detection voltages (V_{dc}) versus input rf frequency at rf input power of 10 μW for devices *A*, *B*, and *C*. The red lines are the Lorentz fitting curves under zero magnetic field for devices *A*, *B*, *C*, respectively. Due to differences in magnetic anisotropy, the antisymmetric part changes while the symmetric part does not. (d)–(f) The STFMR curves of device *A*, *B*, and *C* under the different rf input powers at $H = 0$ Oe. (g)–(i) The rectified voltage as a function of input microwave power for devices *A*, *B*, and *C* at different fixed microwave frequencies.

magnetic field due to the ω_i as a function of the difference between the resonance frequency and the input frequency.

Figure 3 demonstrates the synaptic operation for one of the three MTJs, which the input microwave frequency is close to the resonance frequency of each device under the zero magnetic field (marked by a black dashed line in Fig. 2). Figures 3(a)–3(c) demonstrate a linear relationship between the rectified voltage and the injected microwave power, and the slope (synaptic weight) is controlled by the magnetic field and can be adjusted to both positive and negative values. Figures 3(d)–3(f) display the consistency of ideal and experimental voltages by comparing the experimental voltage with the ideal voltage obtained from the synaptic operation. Thus, we have confirmed that for a single MTJ with PMA, it is possible to demonstrate synaptic operation on a single input signal.

Finally, we used experimental data to perform rf signal classification with an ANN model as shown in Fig. 4. We have created a dataset of simulated rf signals, which corresponds to the input microwave frequency and power in

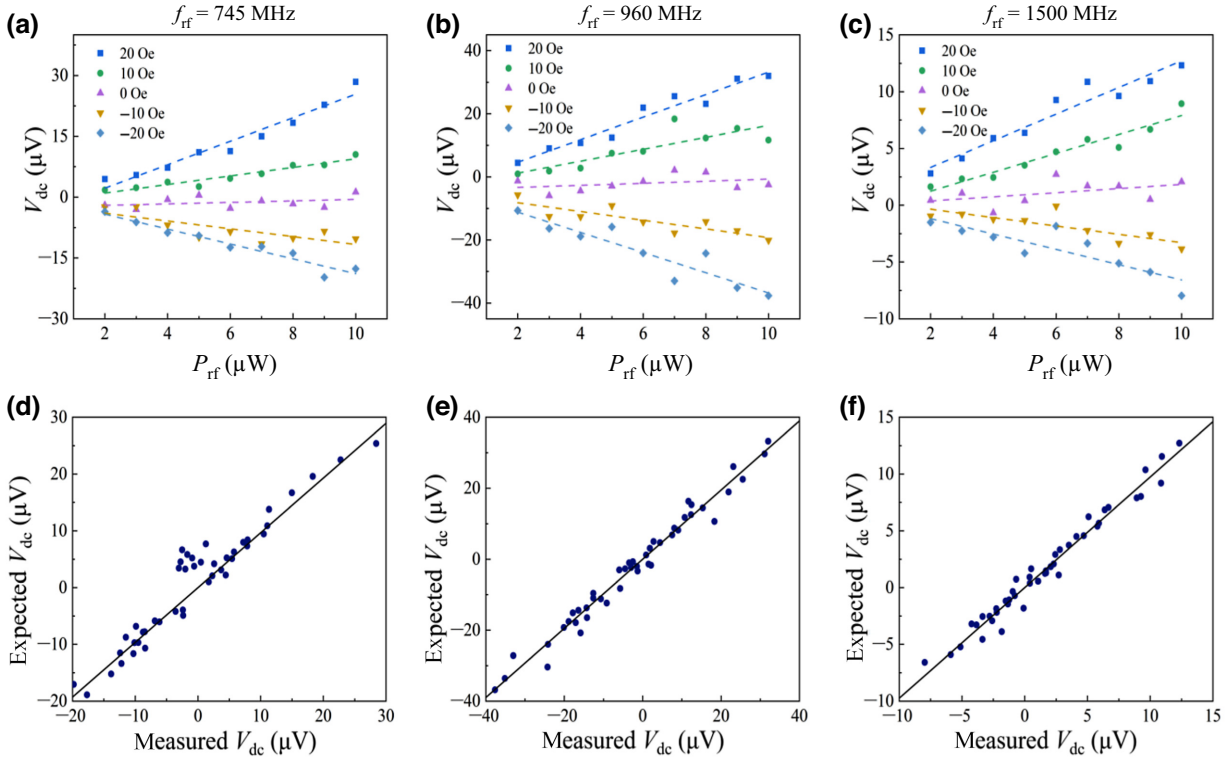

FIG. 3. (a)–(c) The V_{dc} versus rf input power for three MTJs under different magnetic fields (colors). The magnetic field is from −20 to +20 Oe. The dots are experimental data while the dashed lines are linear fits. (d)–(f) compare the experimental voltage with the ideal voltage obtained from the synaptic operation.

Fig. 3, and each sample in the dataset consists of three signals with different frequencies. In our classification model, the purpose of the different frequencies of the signals is to ensure that they are processed by MTJs with corresponding resonance frequencies, with input powers of different signals corresponding to coded information for the desired classification. In our system, signals with input power among 2–5 μW are considered weak signals, and signals with input power among 7–10 μW are considered strong signals. We divided the dataset into three categories, one corresponding to one strong signal and the remaining two corresponding to weak signals, referred to as class 1, class 2, and class 3 (it can be used to represent the three primary colors). For example, in both sample (2, 7, 3) and

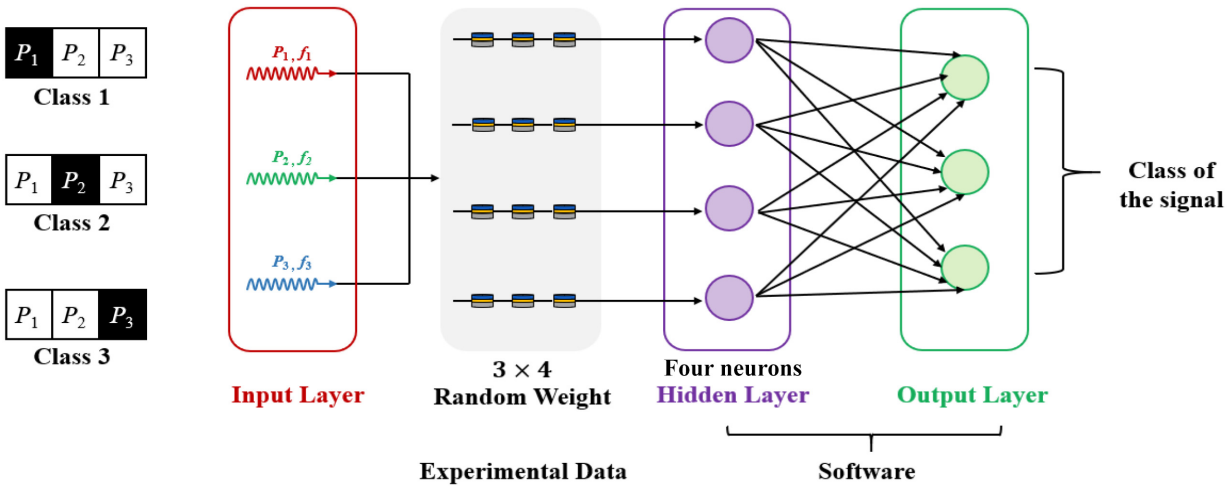

FIG. 4. Schematic of classification by 3 × 4 × 3 ANN model.

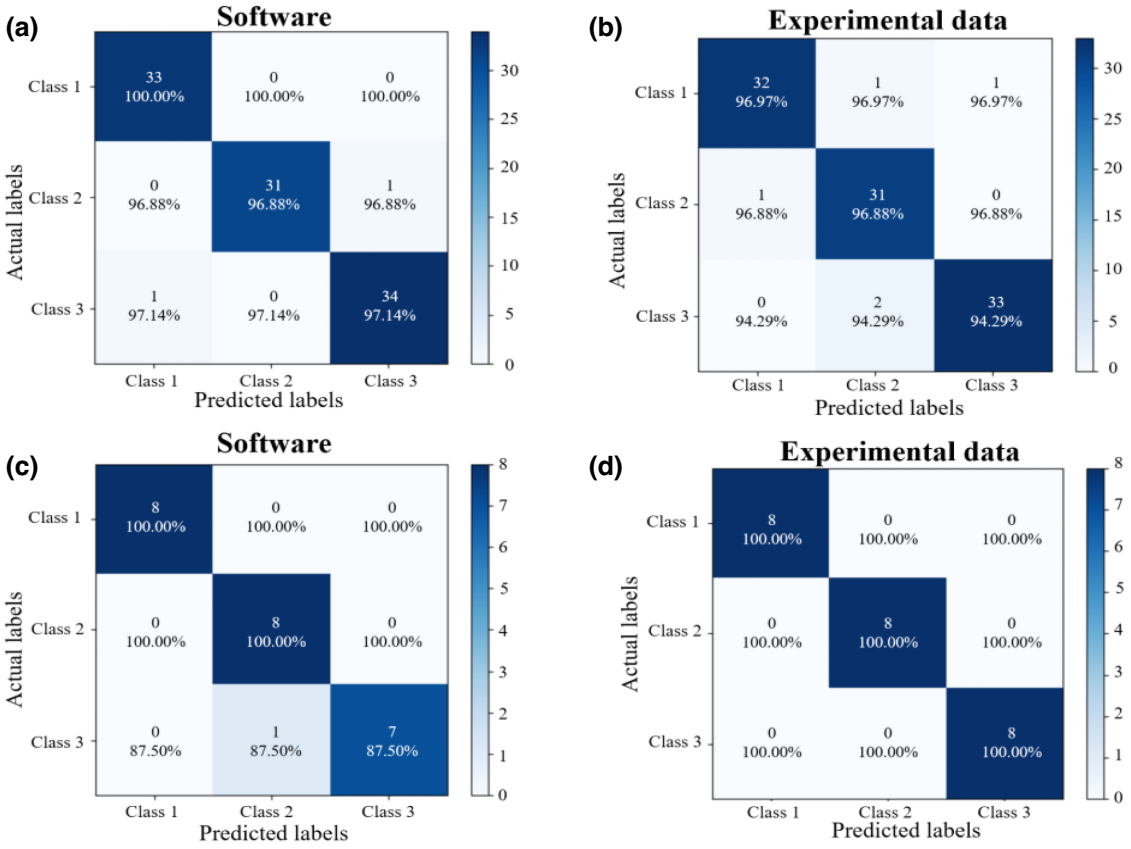

FIG. 5. Confusion matrix for the classification. (a),(b) Training set and (c),(d) testing set both for the software network and for the network using experimental data.

sample (1, 9, 4), the second number is strong signal, so both samples belong to class 2. And our neural network can categorize these samples in the dataset accurately.

We have constructed a "$3 \times 4 \times 3$" neural-network model to classify the signal into three different categories. In this model, the input layer is separated from the output layer by a layer of hidden neurons, and first layer of synapses between the input layer and hidden layer is implemented in four parallel series of three MTJ hardwares. The three MTJs in series corresponded to the devices *A*, *B*, *C* (i.e., following the synapse weights obtained from the experimental data), and the MTJs in parallel were identical. The neurons in the hidden layer, the synaptic weights from the hidden layer to the output layer, and the neurons in the output layer were implemented by means of software methods. Since there were five different weights for each of the MTJs obtained from Fig. 4, we constructed 125 pseudorandom weighted sums. During the training process, we used backpropagation to update the weights, where the weight values in the hidden layer to the output layer were directly adopted from the optimized data, while the synaptic weights between the input layer and the hidden layer were selected from the available experimental data, which were the closest to the optimized data as the real synaptic weights. Then, we processed the rectified voltage values corresponding to different weights in software to get the output result.

During the process, we used a total of 100 training sets for 50 iterations and validated with 24 test sets. In addition, we simultaneously operated with a software-generated neural network. The results show that the accuracy rate of our training set was 96% and test set was 100%, close to the accuracy rates of the software-generated neural network with 98% and 95.83%, respectively. The confusion matrices obtained for the test and training sets are shown in Fig. 5. These results indicate that the neural network using MTJ as a synapse can classify analog signals with an accuracy comparable to a software network.

IV. CONCLUSIONS

In summary, we have demonstrated the MTJs with different resonance through engineering the different PMA between the Co-Fe-B free layer and the MgO tunnel barrier, allowing for selective responses to input signals of different frequencies and enabling multiple analog rf inputs to be processed in parallel. Furthermore, we have confirmed the MTJs with PMA can perform

the synaptic operations with adjustable positive and negative weights, and hold great potential in constructing rf-oriented hardware-implemented ANN. Using uniform mode MTJs with the PMA as synapses, it is easy to obtain MTJs with wider response frequency range to enable the frequency division-multiplexing and rf process. Compared to the method of changing resonance frequency by magnetic field, the modulation using different free-layer thicknesses can reduce energy consumption. This approach allows the parallel processing of rf signals across a wide frequency range and the execution of artificial-intelligence tasks without digitization, which can help reduce costs and energy consumption.

ACKNOWLEDGMENTS

The work was supported by the National Natural Science Foundation of China (Grants No. 12204357, No. 11974379, No. 52371206), the Natural Science Research of Jiangsu Higher Education Institutions of China (Grant No. 22KJB140017), Jiangxi Province "Double Thousand Plan" (Grant No. S2019CQKJ2638). This study was also supported by the CAS Young Talent program.

[1] N. Locatelli, V. Cros, and J. Grollier, Spin-torque building blocks, Nat. Mater. **13**, 11 (2014).

[2] J. Grollier, D. Querlioz, and M. D. Stiles, Spintronic nanodevices for bioinspired computing, Proc. IEEE **104**, 2024 (2016).

[3] J. Torrejon, M. Riou, F. A. Araujo, S. Tsunegi, G. Khalsa, D. Querlioz, P. Bortolotti, V. Cros, K. Yakushiji, A. Fukushima, H. Kubota, S. Yuasa, M. D. Stiles, and J. Grollier, Neuromorphic computing with nanoscale spintronic oscillators, Nature **547**, 428 (2017).

[4] M. A. Zidan, J. P. Strachan, and W. D. Lu, The future of electronics based on memristive systems, Nat. Electron. **1**, 22 (2018).

[5] M. Romera, P. Talatchian, S. Tsunegi, F. Abreu Araujo, V. Cros, P. Bortolotti, J. Trastoy, K. Yakushiji, A. Fukushima, H. Kubota, S. Yuasa, M. Ernoult, D. Vodenicarevic, T. Hirtzlin, N. Locatelli, D. Querlioz, and J. Grollier, Vowel recognition with four coupled spin-torque nano-oscillators, Nature **563**, 230 (2018).

[6] J. Pei, *et al.*, Towards artificial general intelligence with hybrid Tianjic chip architecture, Nature **572**, 106 (2019).

[7] W. A. Borders, A. Z. Pervaiz, S. Fukami, K. Y. Camsari, H. Ohno, and S. Datta, Integer factorization using stochastic magnetic tunnel junctions, Nature **573**, 390 (2019).

[8] H. Jarollahi, N. Onizawa, V. Gripon, N. Sakimura, T. Sugibayashi, T. Endoh, H. Ohno, T. Hanyu, and W. J. Gross, A nonvolatile associative memory-based context-driven search engine using 90 nm CMOS/MTJ-hybrid logic-in-memory architecture, IEEE J. Emerg. Sel. Top. Circuits Syst. **4**, 460 (2014).

[9] S. Lequeux, J. Sampaio, V. Cros, K. Yakushiji, A. Fukushima, R. Matsumoto, H. Kubota, S. Yuasa, and J. Grollier, A magnetic synapse: Multilevel spin-torque memristor with perpendicular anisotropy, Sci. Rep. **6**, 31510 (2016).

[10] Y. Ma, S. Miura, H. Honjo, S. Ikeda, T. Hanyu, H. Ohno, and T. Endoh, A 600-μW ultra-low-power associative processor for image pattern recognition employing magnetic tunnel junction-based nonvolatile memories with autonomic intelligent power-gating scheme, Jpn. J. Appl. Phys. **55**, 04EF15 (2016).

[11] A. Chanthbouala, R. Matsumoto, J. Grollier, V. Cros, A. Anane, A. Fert, A. V. Khvalkovskiy, K. A. Zvezdin, K. Nishimura, Y. Nagamine, H. Maehara, K. Tsunekawa, A. Fukushima, and S. Yuasa, Vertical-current-induced domain-wall motion in MgO-based magnetic tunnel junctions with low current densities, Nat. Phys. **7**, 626 (2011).

[12] S. Li, J. Cai, W. Lv, L. Zhang, S. Liang, and Z. Zeng, Non-volatile logic device based on domain-wall motion in a biaxial magnetic tunnel junction, Jpn. J. Appl. Phys. **60**, 232406 (2021).

[13] W. Lv, J. Cai, H. Tu, L. Zhang, R. Li, Z. Yuan, G. Finocchio, S. Li, X. Sun, L. Bian, B. Zhang, R. Xiong, and Z. Zeng, Stochastic artificial synapses based on nanoscale magnetic tunnel junction for neuromorphic applications, Appl. Phys. Lett. **121**, 020904 (2022).

[14] A. H. Lone and H. Fariborzi, Skyrmion-magnetic tunnel junction synapse with long-term and short-term plasticity for neuromorphic computing, IEEE Trans. Electron Devices **70**, 371 (2023).

[15] N. Leroux, D. Marković, E. Martin, T. Petrisor, D. Querlioz, A. Mizrahi, and J. Grollier, Radio-frequency multiply-and-accumulate operations with spintronic synapses, Phys. Rev. Appl. **15**, 034067 (2021).

[16] A. M. Nathan Leroux, Danijela Marković, Dédalo Sanz-Hernández, Juan Trastoy, Paolo Bortolotti, Leandro Martins, Alex Jenkins, Ricardo Ferreira, and Julie Grollier, Hardware realization of the multiply and accumulate operation on radio-frequency signals with magnetic tunnel junctions, Neuromorphic Comput. Eng. **1**, 011001 (2021).

[17] Nathan Leroux, Arnaud De Riz, Dédalo Sanz-Hernández, Danijela Marković, Alice Mizrahi, and Julie Grollier, Convolutional neural networks with radio-frequency spintronic nano-devices, Neuromorphic Comput. Eng. **2**, 034002 (2022).

[18] A. Ross, *et al.*, Multilayer spintronic neural networks with radio-frequency connections, Nat. Nanotechnol. **18**, 1 (2023).

[19] A. A. Tulapurkar, Y. Suzuki, A. Fukushima, H. Kubota, H. Maehara, K. Tsunekawa, D. D. Djayaprawira, N. Watanabe, and S. Yuasa, Spin-torque diode effect in magnetic tunnel junctions, Nature **438**, 339 (2005).

[20] J. C. Sankey, P. M. Braganca, A. G. Garcia, I. N. Krivorotov, R. A. Buhrman, and D. C. Ralph, Spin-transfer-driven ferromagnetic resonance of individual nanomagnets, Phys. Rev. Lett. **96**, 227601 (2006).

[21] V. S. Pribiag, I. N. Krivorotov, G. D. Fuchs, P. M. Braganca, O. Ozatay, J. C. Sankey, D. C. Ralph, and R. A. Buhrman, Magnetic vortex oscillator driven by d.c. spin-polarized current, Nat. Phys. **3**, 498 (2007).

[22] A. Dussaux, A. V. Khvalkovskiy, P. Bortolotti, J. Grollier, V. Cros, and A. Fert, Field dependence of

spin-transfer-induced vortex dynamics in the nonlinear regime, Phys. Rev. B **86**, 014402 (2012).

[23] E. Grimaldi, A. Dussaux, P. Bortolotti, J. Grollier, G. Pillet, A. Fukushima, H. Kubota, K. Yakushiji, S. Yuasa, and V. Cros, Response to noise of a vortex based spin transfer nano-oscillator, Phys. Rev. B **89**, 104404 (2014).

[24] S. Ikeda, K. Miura, H. Yamamoto, K. Mizunuma, H. D. Gan, M. Endo, S. Kanai, J. Hayakawa, F. Matsukura, and H. Ohno, A perpendicular-anisotropy CoFeB-MgO magnetic tunnel junction, Nat. Mater. **9**, 721 (2010).

[25] P. Khalili Amiri, Z. M. Zeng, J. Langer, H. Zhao, G. Rowlands, Y. J. Chen, I. N. Krivorotov, J. P. Wang, H. W. Jiang, J. A. Katine, Y. Huai, K. Galatsis, and K. L. Wang, Switching current reduction using perpendicular anisotropy in CoFeB–MgO magnetic tunnel junctions, Appl. Phys. Lett. **98**, 112507 (2011).

[26] Z. Zeng, P. K. Amiri, I. N. Krivorotov, H. Zhao, G. Finocchio, J. Wang, J. A. Katine, Y. M. Huai, J. Langer, K. Galatsis, K. L. Wang, and H. Jiang, High-power coherent microwave emission from magnetic tunnel junction nano-oscillators with perpendicular anisotropy, ACS Nano **6**, 6115 (2012).

[27] Z. Zeng, G. Finocchio, B. Zhang, P. Khalili Amiri, J. A. Katine, I. N. Krivorotov, Y. Huai, J. Langer, B. Azzerboni, K. L. Wang, and H. Jiang, Ultralow-current-density and bias-field-free spin-transfer nano-oscillator, Sci. Rep. **3**, 1426 (2013).

[28] O. V. Prokopenko, I. N. Krivorotov, E. Bankowski, T. Meitzler, S. Jaroch, V. S. Tiberkevich, and A. N. Slavin, Spin-torque microwave detector with out-of-plane precessing magnetic moment, J. Appl. Phys. **111**, 123904 (2012).

[29] M. Tarequzzaman, A. S. Jenkins, T. Böhnert, J. Borme, L. Martins, E. Paz, R. Ferreira, and P. P. Freitas, Broadband voltage rectifier induced by linear bias dependence in CoFeB/MgO magnetic tunnel junctions, Appl. Phys. Lett. **112**, 252401 (2018).

[30] B. Fang, M. Carpentieri, S. Louis, V. Tiberkevich, A. Slavin, I. N. Krivorotov, R. Tomasello, A. Giordano, H. Jiang, J. Cai, Y. Fan, Z. Zhang, B. Zhang, J. A. Katine, K. L. Wang, P. K. Amiri, G. Finocchio, and Z. Zeng, Experimental demonstration of spintronic broadband microwave detectors and their capability for powering nanodevices, Phys. Rev. Appl. **11**, 014022 (2019).

[31] L. Zhang, B. Fang, J. Cai, W. Wu, B. Zhang, B. Wang, P. K. Amiri, G. Finocchio, and Z. Zeng, Enhanced broadband radio frequency detection in nanoscale magnetic tunnel junction by interface engineering, ACS Appl. Mater. Interfaces **11**, 29382 (2019).

[32] M. Endo, S. Kanai, S. Ikeda, F. Matsukura, and H. Ohno, Electric-field effects on thickness dependent magnetic anisotropy of sputtered $MgO/Co_{40}Fe_{40}B_{20}/Ta$ structures, Appl. Phys. Lett. **96**, 212503 (2010).

[33] H. Kubota, A. Fukushima, K. Yakushiji, T. Nagahama, S. Yuasa, K. Ando, H. Maehara, Y. Nagamine, K. Tsunekawa, D. D. Djayaprawira, N. Watanabe, and Y. Suzuki, Quantitative measurement of voltage dependence of spin-transfer torque in MgO-based magnetic tunnel junctions, Nat. Phys. **4**, 37 (2008).

[34] J. C. Sankey, Y.-T. Cui, J. Z. Sun, J. C. Slonczewski, R. A. Buhrman, and D. C. Ralph, Measurement of the spin-transfer-torque vector in magnetic tunnel junctions, Nat. Phys. **4**, 67 (2007).

[35] R. Matsumoto, A. Chanthbouala, J. Grollier, V. Cros, A. Fert, K. Nishimura, Y. Nagamine, H. Maehara, K. Tsunekawa, A. Fukushima, and S. Yuasa, Spin-torque diode measurements of MgO-based magnetic tunnel junctions with asymmetric electrodes, Appl. Phys. Express **4**, 063001 (2011).

[36] S. Kanai, M. Gajek, D. C. Worledge, F. Matsukura, and H. Ohno, Electric field-induced ferromagnetic resonance in a CoFeB/MgO magnetic tunnel junction under dc bias voltages, Appl. Phys. Lett. **105**, 242409 (2014).

[37] T. Nozaki, Y. Shiota, S. Miwa, S. Murakami, F. Bonell, S. Ishibashi, H. Kubota, K. Yakushiji, T. Saruya, A. Fukushima, S. Yuasa, T. Shinjo, and Y. Suzuki, Electric-field-induced ferromagnetic resonance excitation in an ultrathin ferromagnetic metal layer, Nat. Phys. **8**, 492 (2012).

[38] J. Zhu, J. A. Katine, G. E. Rowlands, Y.-J. Chen, Z. Duan, J. G. Alzate, P. Upadhyaya, J. Langer, P. K. Amiri, K. L. Wang, and I. N. Krivorotov, Voltage-induced ferromagnetic resonance in magnetic tunnel junctions, Phys. Rev. Lett. **108**, 197203 (2012).

[39] C. Kittel, *Introduction to Solid State Physics* (Wiley, New York, 2005).